

StableQ: Enhancing Data-Scarce Quantization with Text-to-Image Data

Yuhang Li, Youngeun Kim, Donghyun Lee, Priyadarshini Panda
 Department of Electrical Engineering, Yale University

New Haven, CT 06511, United States

{yuhang.li, youngeun.kim, donghyun.lee, priya.panda}@yale.edu

Abstract

Though low-bit quantization enables efficient storage and inference of deep neural networks, it often requires the use of training data to maintain resilience against quantization errors. However, training data are frequently subject to privacy or copyright concerns. In this work, we address the challenge of Data-Scarce Quantization, where access to training data is severely limited or non-existent for quantization purposes. Conventional approaches typically rely on inverting dummy images or jointly training generative models to produce synthetic input samples. However, these methods struggle to accurately recreate complex objects in large-scale datasets like ImageNet. To overcome these limitations, we introduce *StableQ*, a novel method that utilizes an advanced text-to-image diffusion model to generate high-resolution, photo-realistic synthetic data. To verify the quality of the generated data, we implement two robust filtering mechanisms. These mechanisms are designed to select images that closely resemble the intrinsic characteristics of the actual training data. Furthermore, in scenarios where limited training data are available, we use these data to guide the synthetic data generation process by inverting a learnable token embedding in the text encoder. Our extensive experimental results demonstrate that *StableQ* sets a new benchmark in both zero-shot and few-shot quantization, outperforming existing methods in terms of accuracy and efficiency.

1. Introduction

A variety of model compression techniques have been developed to enable the deployment of deep learning models on embedded/mobile devices without significant performance loss. One prominent method is neural network quantization [22], which involves converting 32-bit floating-point models into compact low-bit fixed-point formats. This transformation leverages the efficiency of fixed-point computation and the benefits of reduced memory usage. Other notable techniques include pruning [6] and knowledge distillation [28], both of which aim to reduce network size



Figure 1. Examples images generated by *StableQ* on ImageNet.

while preserving as much of the original model’s performance as possible.

While these methods effectively accelerate neural networks, they typically require finetuning on the original training dataset to mitigate any accuracy loss in the compressed model. However, accessing the original training data can be challenging due to privacy concerns or Intellectual Property (IP) protection issues [47]. This challenge has led to the emergence of *data-free quantization* [8, 25, 37] (also known as zero-shot quantization). This approach involves generating synthetic data from a pretrained network and then finetuning the compressed or quantized model using this synthetic data, thereby circumventing the need for original training data.

Several prior works generate synthetic data by inverting the knowledge from pretrained full-precision models. For instance, [8, 25, 72] propose to optimize the images by aligning them with the training data in terms of activation statistics. [43, 65] apply generative adversarial networks [24] to synthesize the images. However, these approaches often struggle to match the compression performance achievable with real training data. The primary challenge lies in the inherent complexity of reverse mapping from a lower to a higher dimension [39]. For example, in the context of the ImageNet dataset, this involves map-

ping from a 1000-dimensional space to an image space of $224 \times 224 \times 3$. Such transformation makes accurately recreating complex objects a hard problem.

In this paper, we introduce *StableQ*, a novel pipeline utilizing the leading open-source text-to-image model, Stable Diffusion [56], to generate high-quality data for finetuning quantized models. This approach aligns with the growing trend of applying AI Generated Content (AIGC) in deep learning and general vision applications [7, 62, 70]. While direct application of text-to-image synthetic data risks distribution shift from original training data, *StableQ* addresses this through two innovative filtering mechanisms, ensuring the selection of in-distribution synthetic data. *StableQ* excels in both zero-shot and few-shot quantization scenarios. In few-shot quantization, where limited training data is available, *StableQ* employs prompt tuning to align synthetic image generation more closely with the real data. This approach marks a significant advancement in quantization-aware training, particularly in data-scarce environments. **Fig. 1** showcases example images generated by *StableQ*, illustrating its efficacy. We conduct comprehensive experiments to validate the effectiveness of *StableQ*, including both Post-Training Quantization (PTQ) and Quantization-Aware Training (QAT), on various neural network architectures (e.g. CNNs [26, 58] and ViTs [16]).

We summarize our contributions as follows:

1. We propose *StableQ*, the first work to leverage advanced text-to-image synthetic data for Data-Scarce Quantization.
2. To reduce the distribution gap between synthetic data and real data, we introduce the energy score filter and the Batch Normalization (BN) sensitivity filter to select in-distribution synthetic data. We also propose to learn the dataset token to bridge the gap between few-shot training data and synthetic data.
3. Extensive experiments demonstrate *StableQ* generates state-of-the-art quality data, achieving the best quantization performance in both PTQ and QAT. For example, our 3-bit QAT-based ResNet-50 achieves 74.0% accuracy on the ImageNet dataset, outperforming the existing method by 48%.

2. Related Work

Quantization Methods. Quantization approaches to compress pretrained Deep Neural Networks (DNNs) can be broadly divided into PTQ and QAT. PTQ performs *calibration* on a pretrained DNN after quantizing its weights and activations to low bits to maintain the original accuracy [19, 45, 49]. For example, [3, 20] propose bias correction in the convolutional layers after quantization. [74] splits the outliers into additional channels to reduce the quantization error. Recently, a line of works [32, 38, 48, 64]

leverages the weight rounding optimization to reconstruct the activation of the original model. While PTQ mostly adopts ad hoc strategies to prevent accuracy loss from quantization, QAT can significantly improve the accuracy of the quantized model through end-to-end finetuning. The success of QAT is mainly based on the usage of Straight-Through Estimator (STE) [68], enabling gradient-based optimization [10, 18, 31, 66, 71, 76]. QAT also explores optimizing the step size [18], clipping threshold [10], non-linear interval [37], non-uniform quantization levels [71] together with the weights.

Data in Quantization. To quantize a model below 8 bits, data is essential, especially in QAT where end-to-end finetuning occurs. When access to real images is restricted due to privacy and copyright issues, zero-shot quantization [8] proposes to synthesize images in replacement of real data. There are two categories of creating synthetic images: (1) Inverting the images directly via gradient descent [8, 25, 36, 39, 72], and (2) Learning a Generative Adversarial Network (GAN) to continuously generate images [43, 65].

The image inversion [67] relies on Batch Normalization (BN) [8, 25] as an optimization metric to distill the data and obtain high-fidelity images. Other inversion methods based on loss function [75], model ensembling [39], and advanced convolutional layers [36] have been proposed to obtain better synthetic data. However, the inversion approach is limited in certain ways: (1) Inverting images adds a significant computation burden, which makes QAT with synthetic data prohibitive; (2) Models that do not have BN layers, such as ViTs, cannot invert images [16]. The second category proposes to use GAN as an image synthesis engine [11, 43, 52, 65, 75]. These works finetune the generator and the quantized model simultaneously.

Our method opens a third category in data-scarce quantization, *i.e.*, using text-to-image diffusion models. We also investigate the few-shot quantization that generates synthetic data given limited training data to better finetune the quantized model. To the best of our knowledge, this scenario is being studied for the first time.

Synthetic Data in Deep Learning. Initial studies, such as those by [5, 35, 73], explored the use of GANs for assisting DNNs in classifier tuning, object segmentation, and contrastive learning. Recently, the emergence of text-to-image models [14, 46, 56, 57] has revolutionized the synthesis of high-quality data in deep learning, owing to their effectiveness and efficiency. For example, [27] utilized GLIDE [50] for image synthesis in classifier tuning on the CLIP model [54]. In a more advanced application, StableRep [62] leverages Stable Diffusion to generate datasets for contrastive learning, using synthetic data from different seeds as positive pairs. Meanwhile, [2] investigates the synthesis of data within the ImageNet label space observ-

ing accuracy improvements. Furthermore, Fill-up [59] employs synthetic data from text-to-image models to balance the long-tail distribution in training datasets.

3. Preliminaries

3.1. Quantization

Uniform quantization maps full-precision weights into fixed-point numbers. For a step size $s \in \mathbb{R}$, the integer value of weights \mathbf{w} are given by

$$\mathbf{w}_{\text{int}} = \text{clip} \left(\left\lfloor \frac{\mathbf{w}}{s} \right\rfloor + \mathbf{z}, n, p \right), \quad (1)$$

where $\lfloor \cdot \rfloor$ denotes the rounding-to-nearest operation, and n and p represent the lower and upper bound of the integers, respectively. For example, under the b -bit uniform quantization, n and p are set to 0 and 2^{b-1} . The zero-point vector \mathbf{z} is an all- z vector, where $z = -\lfloor \frac{\min(\mathbf{w})}{s} \rfloor$. Thus, the quantized weights \mathbf{w}^q are given by

$$\mathbf{w}^q = s(\mathbf{w}_{\text{int}} - \mathbf{z}). \quad (2)$$

There are several algorithms to determine the step size s , depending on the specific quantization regime. For instance, under QAT, we utilize the LSQ [18] to update the step size with gradient descent. The gradient to step size can be computed with STE [68], *i.e.*, $\frac{\partial \lfloor x \rfloor}{\partial x} = 1$. However, under the PTQ regime, the training data is much less than QAT, hindering the learning of step size. To obtain the desired step size under PTQ, we can use the min-max algorithm or quantization-error minimization [3]. In addition, we also optimize weight rounding during PTQ [36, 38, 48, 64], which can significantly improve the model performance.

3.2. DDPM

The Denoising Diffusion Probabilistic Model (DDPM) [29] is a fundamental component of today’s text-to-image models. The DDPM is a parameterized Markov chain, iteratively denoising the noisy images with finite transition steps. During training, the transition kernels are learnt in the reverse direction to perturbing natural images with noise. The noise is added to the data in each step and estimated as the optimization target.

Forward Process. We briefly introduce the Markov process where Gaussian noise is added to the clean image at each step till it is completely randomized. Given a data distribution $\mathbf{x}_0 \sim q(\mathbf{x}_0)$, DDPM generates \mathbf{x}_T iteratively with $q(\mathbf{x}_T | \mathbf{x}_{T-1})$, given by

$$q(\mathbf{x}_{1:T} | \mathbf{x}_0) = \prod_{t=1}^T q(\mathbf{x}_t | \mathbf{x}_{t-1}), \quad (3)$$

where $q(\mathbf{x}_t | \mathbf{x}_{t-1}) := \mathcal{N}(\mathbf{x}_t; \sqrt{1 - \beta} \mathbf{x}_{t-1}, \beta I)$. T is number of diffusion steps and β is a hyper-parameter to control the perturbation. \mathcal{N} is the Gaussian noise transition kernel.

Reverse Process. Now we can train the transition kernel with a reverse process. Let θ denote its parameters, we predict the generated distribution $p_\theta(\mathbf{x}_0)$ starting from $p_\theta(\mathbf{x}_T)$. The optimization objective is given by

$$\min_{\theta} \mathbb{E}_{t \sim \mathcal{U}(1, T), \mathbf{x}_0 \sim q(\mathbf{x}_0), \epsilon \sim \mathcal{N}(\mathbf{0}, \mathbf{I})} \lambda(t) \|\epsilon - \epsilon_\theta(\mathbf{x}_t, t)\|_F^2, \quad (4)$$

where $\lambda(t)$ is a positive weighting function [29], ϵ is a noise vector predicted from \mathbf{x}_t , and ϵ_θ represents a deep neural network with parameter θ . In this work, we mainly adopt the Stable Diffusion [60], one of the leading open-sourced text-to-image models. In addition to DDPM, the Stable Diffusion further improves the data quality and reduces the complexity by performing diffusion and denoising in the latent space. It uses a VQ-GAN [17] to encode the image into the latent space and decode the latent image after denoising. Also, Stable Diffusion uses cross-model attention to generate images under various forms of conditions like text and images. In *StableQ*, we mainly adopt Stable Diffusion v1-5 to synthesize the images.

4. Methodology

In this section, we introduce our methodology to synthesize the training data with Stable Diffusion. We discuss two scenarios in data-scarce quantization: (1) **Zero-Shot Quantization** (ZSQ) where only the label space and a pretrained full-precision model are provided, and (2) **Few-Shot Quantization** (FSQ) where limited training data is provided in addition to the pretrained model and label space. For ZSQ, we consider both PTQ and QAT, while for FSQ, we consider only QAT. We first discuss *StableQ*’s data generation method under ZSQ and FSQ and then introduce the quantization techniques used in *StableQ*.

4.1. Zero-Shot *StableQ*

We propose a *label prompt* method that only uses the label as the prompt to synthesize the images without accessing the pretrained model. For example, for an ImageNet-pretrained model [13], we can synthesize the image based on 1000 class names.

$$\text{Prompt} = \text{"A photo of a } \{\mathbf{D}\} \ \{\mathbf{C}\}" \quad (5)$$

where $\{\mathbf{D}\}$ is a template adjective (*e.g.*, “nice, dark, small”) derived from the CLIP ImageNet template [54]¹. $\{\mathbf{C}\}$ is a randomly chosen class label name. As an example, suppose we choose the class `hamster`, then a random prompt can be generated as “A photo of a clean hamster”. Subsequently, we directly use the text-to-image model like Stable Diffusion to synthesize the data.

In our *label prompt* method, we generate the images relying solely on the label name of each class and the ability of

¹We list the full template in Appendix A

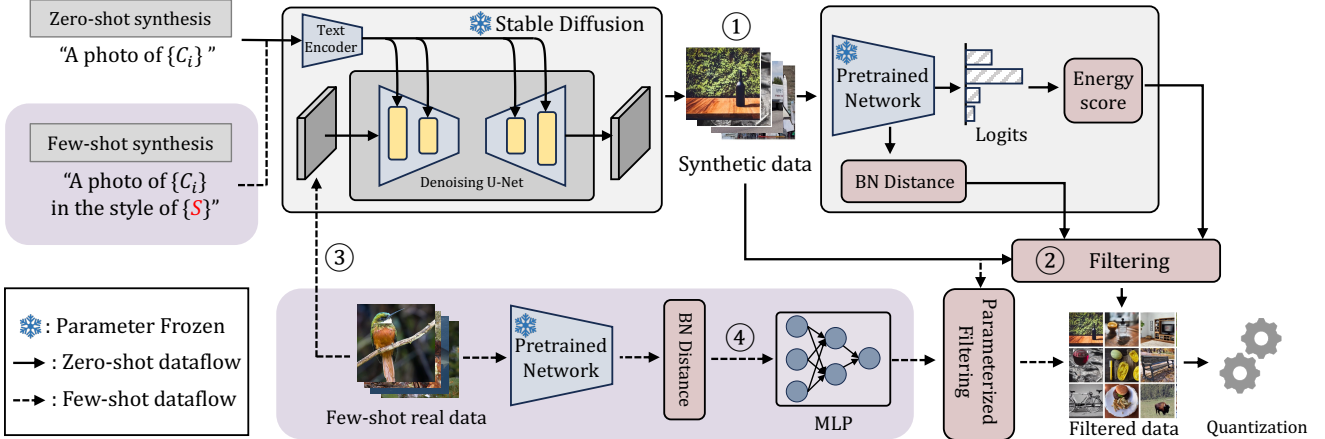


Figure 2. The overall image synthesis and filtering procedure of *StableQ*. ① For zero-shot synthesis, we first generate synthetic images from the stable diffusion. ② Based on the generated synthetic images, we compute BN distance and Energy score, then use them for filtering out low-quality images. ③ For few-shot synthesis, few-shot real images are used to optimize prompt $\{\mathbf{S}\}$ (Eq. (10)). We then generate the synthetic images from the stable diffusion with the optimized prompt. ④ We utilize the BN distance to train a simple MLP model for filtering images, called Parameterized Filtering.

Stable Diffusion (Fig. 2①). However, this operation does not leverage any prior knowledge in the original training data. As a result, the generated image would not be accurate if the target dataset has a large domain gap with the training data of Stable Diffusion or if the label annotation in the target dataset cannot accurately describe the objects. To generate better-quality data for quantization, we propose *model-dependent selection* to leverage the prior knowledge embedded in the pretrained full-precision model.

We propose two filtering mechanisms for model-dependent selection. We argue that the synthetic data selection can be treated as an Out-of-Distribution (OOD) detection problem [51]. However, contrary to OOD detection, we try to select in-distribution data among the synthetic data for quantization purposes (Fig. 2②).

Energy Filtering. We use energy filtering, which calculates the energy score [42], given by

$$E(\mathbf{x}, f) = -T \sum_{i=1}^C e^{-f_i(\mathbf{x})/T}, \quad (6)$$

where $f_i(\mathbf{x})$ denotes the i -th value of the network's output logits. C and T denote the number of image classes and temperature, respectively. Liu *et al.* [42] have shown that the energy score can be used as an OOD detector due to its theoretical connection with the likelihood function. The neural networks trained by cross-entropy loss inherently decrease the energy of the training data, hence, the OOD data will have relatively higher energy.

To select synthetic images that have a similar quantization effect to that of real image data, we pass the synthetic data through the full-precision pretrained model. Then, we

calculate the energy scores of all synthetic images and only select those images for quantization that yield energy scores lower than a certain user-defined threshold. We will experiment with the choice of this threshold in Sec. 5.6.

BatchNorm Distribution Filtering. Originally proposed in [8, 67], the channel mean and channel variance distance computed in the Batch Normalization (BN) layers [34] are regarded as a golden metric for optimizing the synthetic data. [15] also shows that the channel mean discrepancy can also be an OOD detector. We use this metric to evaluate the distance between synthetic images and original training images on the full-precision pretrained model. We calculate the BN distance by

$$D_{BN} = \sum_{\ell=1}^n (||\mu_\ell^s - \mu_\ell||_F + ||\sigma_\ell^s - \sigma_\ell||_F), \quad (7)$$

where μ_ℓ, σ_ℓ denote the running mean and variance of the layer ℓ activation from original training images, and $\mu_\ell^s, \sigma_\ell^s$ are the current mean and variance of the layer ℓ activation from synthetic images. Naively, for each generated synthetic data, we can evaluate the BN distance D_{BN} and filter out the ones with large D_{BN} . However, we find this approach does not bring improvement in the final data quality due to the difference between single data and batched data. Evaluating D_{BN} on a single image will lead to biased estimation as it ignores its interaction with other data. Ioffe [33] also demonstrates that with small batch sizes, the estimates of the batch mean and variance used during training become a less accurate approximation of the mean and variance used for testing.

To deal with this problem, we define a *BN sensitivity*

metric, which measures the independence of one image from other images in a batch. Formally, given a batch of input images $\{\mathbf{x}_i\}_{i=1}^B$ where B indicates the batch size, we define the BN sensitivity of the i -th image $S(\mathbf{x}_i)$ as

$$S(\mathbf{x}_i) = D_{BN}(\{\mathbf{x}_j\}_{j=1}^B) - D_{BN}(\{\mathbf{x}_j\}_{j=1, j \neq i}^B). \quad (8)$$

Here, the BN sensitivity indicates the change in BN distance after removing the selected image. As such, a large BN sensitivity means the current image could potentially damage the internal distribution when it is batched with other images.

Patch Similarity Filtering for ViTs. As we discussed in Sec. 2, since ViTs do not have BN layers, we adopt the patch similarity metric in [40] to do additional filtering of the synthetic images after the energy filtering. ViT quantization is then performed using the filtered synthetic data. We refer to this metric in the Appendix.

4.2. Few-shot *StableQ*

In this section, we describe how to synthesize and select synthetic data given a limited amount of training data (*i.e.*, few-shot quantization). This case could be more common than the completely zero-shot scenario as in practice it is not hard to obtain some permitted training data. We hypothesize that synthesizing a number of images based on this limited dataset can enhance quantization performance.

Considering the ImageNet-1k dataset [13] as the original training dataset, we assume that one image per class (*i.e.*, 1-shot) can be accessed by the cloud server. In this case, we propose to synthesize the images utilizing the existing information from the training data. Specifically, we optimize a text token embedding $\{\mathbf{S}\}$ with the prompt shown below

$$\text{Prompt}_{[i]} = \text{"A photo of a } \{\mathbf{C}_{[i]}\}, \\ \text{in the style of } \{\mathbf{S}\} \text{"}. \quad (9)$$

Here, the learnable token embedding $\{\mathbf{S}\}$ indicates the dataset characteristics of ImageNet. To optimize this learnable token embedding, we associate each class name and the corresponding image into pairs $(\{\mathbf{C}_{[i]}\}, \mathbf{x}_{[i]})$, where $[i]$ is the class index), and let the Stable Diffusion generate $\mathbf{x}_{[i]}$ given $\text{Prompt}_{[i]}$. The optimization objective is given by:

$$\mathbb{E}_{t \sim \mathcal{U}(1, T), i \sim \mathcal{U}(1, M), \epsilon \sim \mathcal{N}(\mathbf{0}, \mathbf{I})} \lambda(t) \|\epsilon - \epsilon_\theta(\mathbf{x}_{[i]t}, t, \text{Prompt}_{[i]})\|_F^2, \quad (10)$$

where M is the number of all object classes. This method is similar to the Textual Inversion [21] which uses a similar technique to learn the token of an object across several images. In contrast to [21], our method learns the token across multiple objects, aiming to characterize the whole dataset. Also, considering that we only have 1 image in each class, performing class-wise Textual Inversion may suffer from over-fitting and generate less diverse data (Fig. 2③).



Figure 3. Visualization of zero/few-shot *StableQ* and real images of *high-speed train* on ImageNet dataset.

Parameterized BatchNorm Distribution Filtering. The previous BN Sensitivity filter in Zero-shot *StableQ* does not require any data. To further enhance the quality of generated data, we leverage the few-shot training data to train a parameterized BN distribution filter (Fig. 2④). As demonstrated in [4], channels in deep neural networks are correlated and of different importance. Hence, instead of simply averaging all BN channels and layers together (*cf.* Eq. (7)), we train a filter model $g(\cdot)$ that takes the BN distance of each layer and outputs whether the image should be kept or removed.

To train this parameterized filter, we leverage the few training data as in-distribution samples and also craft out-of-distribution samples by randomly permuting the pixels of the training data. As a result, we optimize the filter to output 1 or 0, which corresponds to in-distribution samples (kept for quantization) or out-of-distribution samples (removed).

The filter is lightweight, using only a simple MLP structure, and can be trained with few input samples to significantly improve the filtering quality. In addition, the inference can be done with image-by-image prediction, *i.e.*, batch size is 1. The overall *StableQ* pipeline is described in Fig. 2 for both zero-shot and few-shot image synthesis.

4.3. *StableQ* Finetuning

To further improve the performance of PTQ models, QAT-based finetuning will be beneficial. In this work, we take the state-of-the-art PTQ pipeline [36, 38, 48] and apply QAT finetuning with *StableQ* generated synthetic data. Specifically, after rounding learning in PTQ, the quantization becomes

$$\mathbf{w}_{\text{int}} = \text{clip} \left(\left\lfloor \frac{\mathbf{w}}{s} \right\rfloor + \text{sgn}(\mathbf{v}) + \mathbf{z}, n, p \right), \quad (11)$$

where $\text{sgn}(\cdot)$ is the sign function indicating rounding up or down. The vector \mathbf{v} is already well-optimized in the PTQ reconstruction stage. To initialize from the PTQ model and stabilize the training process, we detach all previous learnable variables including \mathbf{w} and \mathbf{v} , and reinitialize an all-zero

Table 1. Evaluation of zero-shot post-training quantization on CNN models (top-1 accuracy (%)).

| Quant. Method | Syn. Method | #Bits (W/A) | ResNet-18 | ResNet-50 | MobileNetV2 | MobileNet-b | MnasNet-1.0 |
|---------------|--------------------------|-------------|--------------|--------------------|--------------|--------------|--------------|
| Full Prec. | N/A | 32/32 | 71.08 | 77.00 | 72.49 | 74.53 | 73.52 |
| BRECQ [38] | Real Data | 4/4 | 69.62 | 75.45 | 68.84 | - | - |
| | ZeroQ [‡] [8] | | 69.32 | 73.73 | 49.83 | 55.93 | 52.04 |
| | KW [‡] [25] | | 69.08 | 74.05 | 59.81 | 61.94 | 55.48 |
| | IntraQ [†] [75] | | 68.77 | 68.16 | 63.78 | - | - |
| | Qimera [11] | | 67.86 | 72.90 | 58.33 | - | - |
| | MixMix [‡] [39] | | 69.46 | 74.58 | 64.01 | 65.38 | 57.87 |
| | GENIE-D | | 69.40 | 75.35 | 67.81 | 64.24 | 65.02 |
| GENIE-M* [36] | <i>StableQ</i> | 4/4 | 69.52 | 75.47 | 68.34 | 67.08 | 66.33 |
| | Real Data | | 69.82 | 75.51 | 69.11 | 69.26 | 68.40 |
| | GENIE-D [36] | | 69.72 | 75.61 | 68.62 | 67.31 | 67.03 |
| BRECQ [38] | <i>StableQ</i> | 2/4 | 69.77 | 75.50 | 68.96 | 68.74 | 68.06 |
| | Real Data | | 65.25 | 70.65 | 54.22 | - | - |
| | ZeroQ [8] | | 61.63 | 64.16 [‡] | 34.39 | 23.53 | 13.83 |
| | KW [‡] [25] | | - | 57.74 | - | - | - |
| | IntraQ [†] [75] | | 55.39 | 44.78 | 35.38 | - | - |
| | Qimera [11] | | 47.80 | 49.13 | 3.73 | - | - |
| | MixMix [‡] [39] | | - | 66.49 | - | - | - |
| GENIE-M* [36] | GENIE-D [36] | 2/4 | 63.93 | 69.72 | 49.75 | 38.01 | 45.53 |
| | <i>StableQ</i> | | 65.04 | 69.90 | 53.08 | 47.31 | 50.84 |
| | Real Data | | 66.05 | 70.96 | 56.42 | 55.00 | 54.66 |
| GENIE-M* [36] | GENIE-D [36] | 2/4 | 64.86 | 69.89 | 51.47 | 47.69 | 48.38 |
| | <i>StableQ</i> | | 65.72 | 70.35 | 54.82 | 52.77 | 52.76 |

[‡] The figures are taken from [39]. [†] It synthesizes 5K images while others synthesize only 1K images.

* Denotes our implementation based on the open-source code, hyper-parameters are kept the same for all data synthesis methods.

vector \mathbf{u} . The new quantization function is thus given by

$$\mathbf{w}_{\text{int}} = \text{clip} \left(\left\lfloor \frac{\mathbf{w}}{s} \right\rfloor + \text{sgn}(\mathbf{v}) + \left\lfloor \frac{\mathbf{u}}{s} \right\rfloor + \mathbf{z}, n, p \right). \quad (12)$$

The de-quantization step remains the same with Eq. (2). By introducing an additional variable \mathbf{u} and detaching the previous variable, we start from the original PTQ model and avoid passing gradient through floor operation. As a result, the \mathbf{u} can be safely updated through STE.

5. Experiments

In this section, we empirically demonstrate the superiority of our *StableQ* synthetic data in both a qualitative and a quantitative way. For the PTQ scenario, we follow the conventional setup [36, 38, 39] to synthesize 1k images. As for the QAT scenarios, we synthesize 1.2M images with 1200 images in each object class to match the original ImageNet dataset. Unless specified, we use Stable Diffusion v1-5 [1] and set the guidance scale to 3.5². We will first provide the visualization of our synthetic data, and then compare them against existing state-of-the-art methods. Finally, we analyze *StableQ* by conducting various ablation and generalization studies.

²*StableQ* generates one image per second on one A100 GPU.

Table 2. Evaluation of zero-shot post-training quantization on ViT models (top-1 accuracy (%)).

| Quant. Method | Syn. Method | #Bits | ViT-B | DeiT-B | Swin-B |
|---------------|----------------|-------|--------------|--------------|--------------|
| Full Prec. | N/A | 32/32 | 84.54 | 81.80 | 85.27 |
| PTQ4ViT [69] | Real Data | 4/4 | 58.07 | 63.57 | 75.20 |
| | PSAQ-ViT [40] | | 60.26 | 65.18 | 72.12 |
| RepQ-ViT [41] | <i>StableQ</i> | 4/4 | 63.17 | 67.08 | 74.27 |
| | Real Data | | 67.93 | 75.99 | 72.80 |
| RepQ-ViT [41] | PSAQ-ViT [40] | 4/4 | 60.18 | 74.69 | 54.21 |
| | <i>StableQ</i> | | 67.50 | 76.10 | 70.08 |

5.1. Analysis on Synthetic Data

As shown in Fig. 1, the *StableQ* images after filtering are high-quality and visually similar to real images. Moreover, to show the effect of our few-shot image generation, we provide an example of *high-speed train* class in the ImageNet dataset [13]. Fig. 3 shows the 1-shot real image, the zero-shot label prompt images, and the few-shot token prompt inversion images. The zero-shot images have more natural sites as background, while the few-shot images generate more in-station views just like the real image.

5.2. Zero-Shot PTQ Evaluation

We evaluate our proposed method by testing it on two types of neural networks, (1) ConvNets such as ResNet [23], MobileNet [30, 58], RegNet [55], and MnasNet [61]

Table 3. Evaluation of zero-shot quantization-aware training CNNs (top-1 accuracy (%)).

| Method | #Real Data | #Syn Data | #Bits (W/A) | ResNet-18 | MobileNetV2 | ResNet-50 |
|----------------------------|------------|-----------|-------------|--------------|--------------|--------------|
| LSQ [18] (ICLR 2020) | 1.2M | 0 | 4/4 | 71.10 | 69.50 | 76.70 |
| GDFQ [65] (ECCV 2020) | 0 | 1.2M | | 60.60 | 59.43 | 54.16 |
| ZAQ [43] (CVPR 2021) | 0 | 4.6M | | 52.64 | 0.10 | 53.02 |
| Qimera [11] (NeurIPS 2021) | 0 | 1.2M | | 63.84 | 61.62 | 66.25 |
| IntraQ [75] (CVPR 2022) | 0 | 5k | | 66.47 | 65.10 | - |
| ARC+AIT [12] (CVPR 2022) | 0 | 1.2M | 4/4 | 65.73 | 66.47 | 68.27 |
| DSG [53] (TPAMI 2023) | 0 | 1.2M | | 62.18 | 60.46 | 71.96 |
| AdaDFQ [52] (CVPR 2023) | 0 | 1.2M | | 66.53 | 65.41 | 68.38 |
| TexQ [9] (NeurIPS 2023) | 0 | 1.2M | | 67.73 | 67.07 | 70.72 |
| <i>StableQ</i> | 0 | 1.2M | | 70.03 | 69.65 | 76.10 |
| LSQ [18] (ICLR 2020) | 1.2M | 0 | 3/3 | 70.20 | 65.30 | 75.80 |
| GDFQ [65] (ECCV 2020) | 0 | 1.2M | | 20.23 | 1.46 | 0.31 |
| AdaDFQ [52] (CVPR 2023) | 0 | 1.2M | | 38.10 | 28.99 | 17.63 |
| TexQ [9] (NeurIPS 2023) | 0 | 1.2M | 3/3 | 50.28 | 32.80 | 25.27 |
| <i>StableQ</i> | 0 | 1.2M | | 68.18 | 59.15 | 73.99 |

and (2) Vision Transformers like original ViT [16]. For CNNs PTQ, we employ the state-of-the-art PTQ algorithms—BRECQ [38] and GENIE-M [36] to perform the W4A4 and W2A4 quantization, which reconstruct the activation output in a block-wise manner. In this case, we use 1024 synthetic images for quantization evaluation. For ViT PTQ, we perform PTQ4ViT [69] and RepQ-ViT [41] across 5 different models, including ViT-M [16], DeiT-M [63], and Swin-B [44]. We follow the open-source code implementation and generate 32 images as the calibration dataset to obtain the quantized ViTs. For all cases, we generate 2× synthetic data and filter 50% of them to match the volume.

Comparison on CNNs. We select existing state-of-the-art image synthesis algorithms as our comparison, including ZeroQ [8], the Knowledge Within [25], IntraQ [75], Qimera [11], MixMix [39], GENIE-D [36]. For reference, we also include the performance of PTQ using 1024 real ImageNet-1k images. We summarize all the accuracy results in Table 1. It can be observed that our *StableQ* achieves the highest accuracy in most cases. Interestingly, we find that the network architecture affects the performance of synthetic data. On ResNet architectures, *StableQ* and GENIE-D have similar accuracy (0.1–0.5%) levels, however, *StableQ* largely outperforms other zero-shot algorithms on lightweight network architectures due to their lower quantization resilience. As an example, *StableQ* increases 5% accuracy compared to GENIE-D on MobileNet-b W2A4 quantization and 4.4% accuracy on MNasNet W2A4 quantization as well.

Comparison on Vision Transformers. Given that there is only one zero-shot algorithm for ViTs, PSAQ-ViT [40], we compare *StableQ* with PSAQ-ViT in Table 2. *StableQ* consistently outperforms PSAQ-ViT [40]. For example, on ViT-B and Swin-B, our method has 7.3% and 15% accu-

Table 4. Evaluation of few-shot quantized ResNet-18 (W3A3).

| Method | #Real Data | #Syn Data | Accuracy |
|----------------|------------|-----------|--------------|
| GENIE-M [36] | 1k | 0 | 67.34* |
| | 1k | 0 | 67.45* |
| | 10k | 0 | 67.94* |
| LSQ [18] | 100k | 0 | 68.32* |
| | 300k | 0 | 69.13* |
| | 1.2M | 0 | 70.20 |
| <i>StableQ</i> | 1k | 1.2M | 68.88 |

* denotes our implementation.

racy improvement using the RepQ-ViT method. This result proves that *StableQ* can achieve state-of-the-art performance on both CNNs and ViTs.

5.3. Zero-shot QAT Evaluation

We then compare *StableQ* with existing generative zero-shot QAT methods, such as GDFQ [65], ZAQ [43], Qimera [11], IntraQ [75], ARC [12], AdaDFQ [52], TexQ [9]. Note that these methods jointly optimize GAN and quantized model. Thus, they can generate *unlimited* synthetic data during finetuning. We originally have 1.6M synthetic images (1600 images/class), and then filter 0.4M (400 images/class) images using the energy filter and the BN distance filter. We use the SGD optimizer with a learning rate of 0.001 followed by a cosine annealing decay schedule for 50 epochs. Additionally, we report the LSQ results using 1.2M real ImageNet data. The results are summarized in Table 3. Our method largely outperforms other zero-shot QAT methods and nearly approaches the accuracy of LSQ baseline. Remarkably, *StableQ* improves the accuracy of W3A3 quantization by a large margin, for instance, *StableQ* exceeds 48% accuracy of TexQ, the best-performing method.

Table 5. Cross-model evaluation on synthetic data. We compare the data transferability between existing (a) and our (b) methods.

| (a) GENIE-D & PSAQ-ViT | | | (b) <i>StableQ</i> | | |
|------------------------|-------|-------|--------------------|-------|-------|
| Source model | Res18 | MBV2 | Source model | Res18 | MBV2 |
| Res18 | 64.86 | 48.37 | Res18 | 65.72 | 54.32 |
| MBV2 | 64.21 | 51.47 | MBV2 | 65.52 | 54.82 |
| ViT-B-16 | 47.27 | 17.96 | ViT-B-16 | 65.44 | 54.24 |

5.4. Few-shot QAT Evaluation

In this section, we evaluate the few-shot QAT scenarios. Our main comparison is LSQ [18] using different amounts of real data. We show how much of the real data can our *StableQ* generated synthetic data match in practice. To ensure a fair comparison, we initialize the QAT model by performing GENIE-M on 1k real data and then finetune the model using $\{1k, 10k, 100k, 300k, 1.2M\}$ real data, corresponding to 1-shot, 10-shot, 100-shot, 300-shot, and full-shot data regimes, respectively. To generate *StableQ* data, we initialize the token embedding as ImageNet, and train it for 50k iterations with a batch size of 8, learning rate set to 5e-4 with Adam optimizer.

As summarized in Table 4, the initialized PTQ model reaches 67.34% accuracy, and the few-shot LSQ increases its accuracy as more real images are provided. QAT with only 1k real images does not bring much improvement (0.1%). The performance of QAT is highly correlated with the number of real data. Finally, despite only using 1-shot real data, *StableQ* is able to achieve approximately 100-shot QAT accuracy.

5.5. Data Transferability Evaluation

[39] has demonstrated that the synthetic data extracted from one model has low transferability on other models, *i.e.*, low data transferability among different models. To demonstrate that *StableQ* has relatively high transferability, we conduct a cross-model evaluation, *e.g.*, synthesizing images based on model A, and test the quantization on model B. In Table 5a we provide the results of GENIE-D and PSAQ-ViT, tested on zero-shot PTQ W2A4 scenarios. We then summarize the results of *StableQ* in Table 5b. We observe that the *StableQ* data, although filtered by a different model, only drops 0.2-0.5% final accuracy, while the existing methods drop 0.6-33% accuracy, especially when using ViT synthetic data for MobileNetV2 quantization.

5.6. Ablation study

In this section, we conduct ablation studies on two variables, (1) the number of synthetic data, and (2) the image filtering strength.

Number of synthetic data in PTQ. In practice, synthesizing images using *StableQ* does not cost a lot of computing resources (1 image/second). Hence, we can safely increase the number of synthetic data with minimal overhead

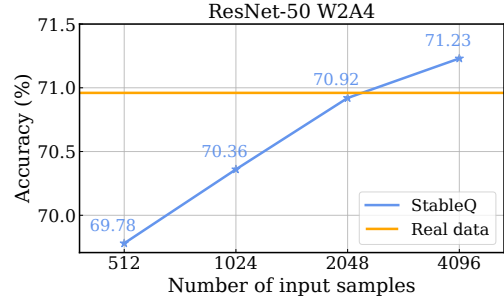


Figure 4. Accuracy vs # synthetic data with zero-shot PTQ.

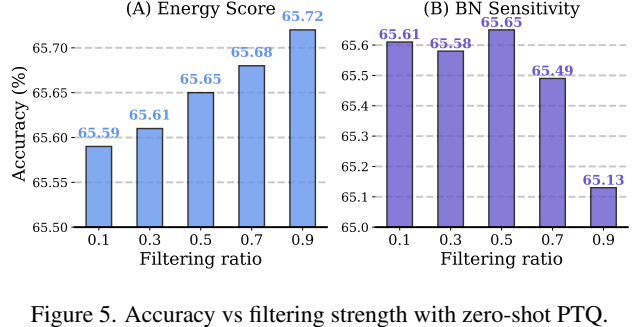


Figure 5. Accuracy vs filtering strength with zero-shot PTQ.

in PTQ cases. Yet retrieving more real data seems much more difficult if the training data is private or under IP protection. In Fig. 4, we show that increasing the synthetic data can consistently improve the PTQ performances of W2A4 quantized ResNet-50. *StableQ* even outperforms real-data baseline when using 4k input images.

Energy Score Filtering Strength. Given a fixed number of synthetic data (N) used for quantization and a percentage r representing how many images are filtered out, the total amount of generated images is $\frac{N}{1-r}$. We test different options of r from $\{0.1, 0.3, 0.5, 0.7, 0.9\}$ to test the effect of energy score filtering. We choose ResNet-18 and use W2A4 zero-shot PTQ for evaluation. The test performance is shown in Fig. 5(A). We generally find that a higher filtering ratio leads to better test accuracy. However, it will also increase the total number of generated images. Nevertheless, the accuracy variation is rather small.

BN Sensitivity Filtering Strength. We run the same test for the BN sensitivity filtering mechanism. The results are shown in Fig. 5(B). Unlike the energy score, setting the ratio to 50% has the best performance, we hypothesize that the networks need more diverse data as stated in [72].

6. Conclusion

In this paper, we have introduced *StableQ*, a novel attempt to synthesize images with text-to-image models for data-scarce quantization. Our *StableQ* generates images in both zero-shot and few-shot regimes and refines the images with several filtering mechanisms and a token embedding learning algorithm. Extensive experiments show that *StableQ* establishes a new state of the art in both PTQ and QAT.

References

- [1] runwayml/stable-diffusion-v1-5 · Hugging Face — huggingface.co. <https://huggingface.co/runwayml/stable-diffusion-v1-5>. [Accessed 13-11-2023]. 6
- [2] Shekoofeh Azizi, Simon Kornblith, Chitwan Saharia, Mohammad Norouzi, and David J Fleet. Synthetic data from diffusion models improves imagenet classification. *arXiv preprint arXiv:2304.08466*, 2023. 2
- [3] Ron Banner, Yury Nahshan, and Daniel Soudry. Post training 4-bit quantization of convolutional networks for rapid-deployment. *Advances in Neural Information Processing Systems*, 32, 2019. 2, 3
- [4] David Bau, Bolei Zhou, Aditya Khosla, Aude Oliva, and Antonio Torralba. Network dissection: Quantifying interpretability of deep visual representations. In *Proceedings of the IEEE conference on computer vision and pattern recognition*, pages 6541–6549, 2017. 5
- [5] Victor Besnier, Himalaya Jain, Andrei Bursuc, Matthieu Cord, and Patrick Pérez. This dataset does not exist: training models from generated images. In *ICASSP 2020-2020 IEEE International Conference on Acoustics, Speech and Signal Processing (ICASSP)*, pages 1–5. IEEE, 2020. 2
- [6] Davis Blalock, Jose Javier Gonzalez Ortiz, Jonathan Franke, and John Guttag. What is the state of neural network pruning? *Proceedings of machine learning and systems*, 2: 129–146, 2020. 1
- [7] Rishi Bommasani, Drew A Hudson, Ehsan Adeli, Russ Altman, Simran Arora, Sydney von Arx, Michael S Bernstein, Jeannette Bohg, Antoine Bosselut, Emma Brunskill, et al. On the opportunities and risks of foundation models. *arXiv preprint arXiv:2108.07258*, 2021. 2
- [8] Yaohui Cai, Zhewei Yao, Zhen Dong, Amir Gholami, Michael W Mahoney, and Kurt Keutzer. Zeroq: A novel zero shot quantization framework. In *Proceedings of the IEEE/CVF Conference on Computer Vision and Pattern Recognition*, pages 13169–13178, 2020. 1, 2, 4, 6, 7
- [9] Xinrui Chen, Yizhi Wang, Renao Yan, Yiqing Liu, Tian Guan, and Yonghong He. Texq: Zero-shot network quantization with texture feature distribution calibration. In *Thirty-seventh Conference on Neural Information Processing Systems*, 2023. 7
- [10] Jungwook Choi, Zhuo Wang, Swagath Venkataramani, Pierce I-Jen Chuang, Vijayalakshmi Srinivasan, and Kailash Gopalakrishnan. Pact: Parameterized clipping activation for quantized neural networks. *arXiv preprint arXiv:1805.06085*, 2018. 2
- [11] Kanghyun Choi, Deokki Hong, Noseong Park, Youngsok Kim, and Jinho Lee. Qimera: Data-free quantization with synthetic boundary supporting samples. *Advances in Neural Information Processing Systems*, 34:14835–14847, 2021. 2, 6, 7
- [12] Kanghyun Choi, Hye Yoon Lee, Deokki Hong, Joonsang Yu, Noseong Park, Youngsok Kim, and Jinho Lee. It's all in the teacher: Zero-shot quantization brought closer to the teacher. In *Proceedings of the IEEE/CVF Conference on Computer Vision and Pattern Recognition*, pages 8311–8321, 2022. 7
- [13] Jia Deng, Wei Dong, Richard Socher, Li-Jia Li, Kai Li, and Li Fei-Fei. Imagenet: A large-scale hierarchical image database. In *2009 IEEE conference on computer vision and pattern recognition*, pages 248–255. Ieee, 2009. 3, 5, 6
- [14] Prafulla Dhariwal and Alexander Nichol. Diffusion models beat gans on image synthesis. *Advances in neural information processing systems*, 34:8780–8794, 2021. 2
- [15] Xin Dong, Junfeng Guo, Ang Li, Wei-Te Ting, Cong Liu, and HT Kung. Neural mean discrepancy for efficient out-of-distribution detection. In *Proceedings of the IEEE/CVF Conference on Computer Vision and Pattern Recognition*, pages 19217–19227, 2022. 4
- [16] Alexey Dosovitskiy, Lucas Beyer, Alexander Kolesnikov, Dirk Weissenborn, Xiaohua Zhai, Thomas Unterthiner, Mostafa Dehghani, Matthias Minderer, Georg Heigold, Sylvain Gelly, et al. An image is worth 16x16 words: Transformers for image recognition at scale. *arXiv preprint arXiv:2010.11929*, 2020. 2, 7, 1
- [17] Patrick Esser, Robin Rombach, and Bjorn Ommer. Taming transformers for high-resolution image synthesis. In *Proceedings of the IEEE/CVF conference on computer vision and pattern recognition*, pages 12873–12883, 2021. 3
- [18] Steven K Esser, Jeffrey L McKinstry, Deepika Bablani, Rathinakumar Appuswamy, and Dharmendra S Modha. Learned step size quantization. *arXiv preprint arXiv:1902.08153*, 2019. 2, 3, 7, 8
- [19] Jun Fang, Ali Shafiee, Hamzah Abdel-Aziz, David Thorsley, Georgios Georgiadis, and Joseph H Hassoun. Post-training piecewise linear quantization for deep neural networks. In *Computer Vision–ECCV 2020: 16th European Conference, Glasgow, UK, August 23–28, 2020, Proceedings, Part II 16*, pages 69–86. Springer, 2020. 2
- [20] Alexander Finkelstein, Uri Almog, and Mark Grobman. Fighting quantization bias with bias. *arXiv preprint arXiv:1906.03193*, 2019. 2
- [21] Rinon Gal, Yuval Alaluf, Yuval Atzmon, Or Patashnik, Amit H Bermano, Gal Chechik, and Daniel Cohen-Or. An image is worth one word: Personalizing text-to-image generation using textual inversion. *arXiv preprint arXiv:2208.01618*, 2022. 5
- [22] Amir Gholami, Sehoon Kim, Zhen Dong, Zhewei Yao, Michael W Mahoney, and Kurt Keutzer. A survey of quantization methods for efficient neural network inference. *arXiv preprint arXiv:2103.13630*, 2021. 1
- [23] Ian Goodfellow, Yoshua Bengio, Aaron Courville, and Yoshua Bengio. *Deep learning*. MIT Press, 2016. 6
- [24] Ian Goodfellow, Jean Pouget-Abadie, Mehdi Mirza, Bing Xu, David Warde-Farley, Sherjil Ozair, Aaron Courville, and Yoshua Bengio. Generative adversarial networks. *Communications of the ACM*, 63(11):139–144, 2020. 1
- [25] Matan Haroush, Itay Hubara, Elad Hoffer, and Daniel Soudry. The knowledge within: Methods for data-free model compression. In *Proceedings of the IEEE/CVF Conference on Computer Vision and Pattern Recognition*, pages 8494–8502, 2020. 1, 2, 6, 7
- [26] Kaiming He, Xiangyu Zhang, Shaoqing Ren, and Jian Sun. Deep residual learning for image recognition. In *Proceed-*

ings of the IEEE conference on computer vision and pattern recognition, pages 770–778, 2016. 2

[27] Ruifei He, Shuyang Sun, Xin Yu, Chuhui Xue, Wenqing Zhang, Philip Torr, Song Bai, and Xiaojuan Qi. Is synthetic data from generative models ready for image recognition? *arXiv preprint arXiv:2210.07574*, 2022. 2

[28] Geoffrey Hinton, Oriol Vinyals, and Jeff Dean. Distilling the knowledge in a neural network. *arXiv preprint arXiv:1503.02531*, 2015. 1

[29] Jonathan Ho, Ajay Jain, and Pieter Abbeel. Denoising diffusion probabilistic models. *Advances in neural information processing systems*, 33:6840–6851, 2020. 3

[30] Andrew G Howard, Menglong Zhu, Bo Chen, Dmitry Kalenichenko, Weijun Wang, Tobias Weyand, Marco Andreetto, and Hartwig Adam. Mobilenets: Efficient convolutional neural networks for mobile vision applications. *arXiv preprint arXiv:1704.04861*, 2017. 6

[31] Itay Hubara, Matthieu Courbariaux, Daniel Soudry, Ran El-Yaniv, and Yoshua Bengio. Quantized neural networks: Training neural networks with low precision weights and activations. *The Journal of Machine Learning Research*, 18(1): 6869–6898, 2017. 2

[32] Itay Hubara, Yury Nahshan, Yair Hanani, Ron Banner, and Daniel Soudry. Improving post training neural quantization: Layer-wise calibration and integer programming. *arXiv preprint arXiv:2006.10518*, 2020. 2

[33] Sergey Ioffe. Batch renormalization: Towards reducing minibatch dependence in batch-normalized models. *Advances in neural information processing systems*, 30, 2017. 4

[34] Sergey Ioffe and Christian Szegedy. Batch normalization: Accelerating deep network training by reducing internal covariate shift. In *International conference on machine learning*, pages 448–456. pmlr, 2015. 4

[35] Ali Jahanian, Xavier Puig, Yonglong Tian, and Phillip Isola. Generative models as a data source for multiview representation learning. *arXiv preprint arXiv:2106.05258*, 2021. 2

[36] Yongkweon Jeon, Chungman Lee, and Ho-young Kim. Geenie: Show me the data for quantization. In *Proceedings of the IEEE/CVF Conference on Computer Vision and Pattern Recognition*, pages 12064–12073, 2023. 2, 3, 5, 6, 7

[37] Sangil Jung, Changyong Son, Seohyung Lee, Jinwoo Son, Jae-Joon Han, Youngjun Kwak, Sung Ju Hwang, and Changkyu Choi. Learning to quantize deep networks by optimizing quantization intervals with task loss. In *Proceedings of the IEEE/CVF Conference on Computer Vision and Pattern Recognition*, pages 4350–4359, 2019. 1, 2

[38] Yuhang Li, Ruihao Gong, Xu Tan, Yang Yang, Peng Hu, Qi Zhang, Fengwei Yu, Wei Wang, and Shi Gu. Brecq: Pushing the limit of post-training quantization by block reconstruction. *arXiv preprint arXiv:2102.05426*, 2021. 2, 3, 5, 6, 7

[39] Yuhang Li, Feng Zhu, Ruihao Gong, Mingzhu Shen, Xin Dong, Fengwei Yu, Shaoqing Lu, and Shi Gu. Mixmix: All you need for data-free compression are feature and data mixing. In *Proceedings of the IEEE/CVF International Conference on Computer Vision*, pages 4410–4419, 2021. 1, 2, 6, 7, 8

[40] Zhikai Li, Liping Ma, Mengjuan Chen, Junrui Xiao, and Qingyi Gu. Patch similarity aware data-free quantization for vision transformers. In *European Conference on Computer Vision*, pages 154–170. Springer, 2022. 5, 6, 7, 1

[41] Zhikai Li, Junrui Xiao, Lianwei Yang, and Qingyi Gu. Repqvit: Scale reparameterization for post-training quantization of vision transformers. In *Proceedings of the IEEE/CVF International Conference on Computer Vision*, pages 17227–17236, 2023. 6, 7

[42] Weitang Liu, Xiaoyun Wang, John Owens, and Yixuan Li. Energy-based out-of-distribution detection. *Advances in neural information processing systems*, 33:21464–21475, 2020. 4

[43] Yuang Liu, Wei Zhang, and Jun Wang. Zero-shot adversarial quantization. In *Proceedings of the IEEE/CVF Conference on Computer Vision and Pattern Recognition*, pages 1512–1521, 2021. 1, 2, 7

[44] Ze Liu, Yutong Lin, Yue Cao, Han Hu, Yixuan Wei, Zheng Zhang, Stephen Lin, and Baining Guo. Swin transformer: Hierarchical vision transformer using shifted windows. In *Proceedings of the IEEE/CVF international conference on computer vision*, pages 10012–10022, 2021. 7

[45] Zhenhua Liu, Yunhe Wang, Kai Han, Wei Zhang, Siwei Ma, and Wen Gao. Post-training quantization for vision transformer. *Advances in Neural Information Processing Systems*, 34:28092–28103, 2021. 2

[46] Andreas Lugmayr, Martin Danelljan, Andres Romero, Fisher Yu, Radu Timofte, and Luc Van Gool. Repaint: Inpainting using denoising diffusion probabilistic models. In *Proceedings of the IEEE/CVF Conference on Computer Vision and Pattern Recognition*, pages 11461–11471, 2022. 2

[47] Abid Mehmood, Iynkaran Natgunanathan, Yong Xiang, Guang Hua, and Song Guo. Protection of big data privacy. *IEEE access*, 4:1821–1834, 2016. 1

[48] Markus Nagel, Rana Ali Amjad, Mart Van Baalen, Christos Louizos, and Tijmen Blankevoort. Up or down? adaptive rounding for post-training quantization. In *International Conference on Machine Learning*, pages 7197–7206. PMLR, 2020. 2, 3, 5

[49] Yury Nahshan, Brian Chmiel, Chaim Baskin, Evgenii Zheltonozhskii, Ron Banner, Alex M Bronstein, and Avi Mendelson. Loss aware post-training quantization. *Machine Learning*, 110(11-12):3245–3262, 2021. 2

[50] Alex Nichol, Prafulla Dhariwal, Aditya Ramesh, Pranav Shyam, Pamela Mishkin, Bob McGrew, Ilya Sutskever, and Mark Chen. Glide: Towards photorealistic image generation and editing with text-guided diffusion models. *arXiv preprint arXiv:2112.10741*, 2021. 2

[51] Marco AF Pimentel, David A Clifton, Lei Clifton, and Lionel Tarassenko. A review of novelty detection. *Signal processing*, 99:215–249, 2014. 4

[52] Biao Qian, Yang Wang, Richang Hong, and Meng Wang. Adaptive data-free quantization. In *Proceedings of the IEEE/CVF Conference on Computer Vision and Pattern Recognition*, pages 7960–7968, 2023. 2, 7

[53] Haotong Qin, Yifu Ding, Xiangguo Zhang, Jiakai Wang, Xianglong Liu, and Jiwen Lu. Diverse sample generation:

Pushing the limit of generative data-free quantization. *IEEE Transactions on Pattern Analysis and Machine Intelligence*, 2023. 7

[54] Alec Radford, Jong Wook Kim, Chris Hallacy, Aditya Ramesh, Gabriel Goh, Sandhini Agarwal, Girish Sastry, Amanda Askell, Pamela Mishkin, Jack Clark, et al. Learning transferable visual models from natural language supervision. In *International conference on machine learning*, pages 8748–8763. PMLR, 2021. 2, 3

[55] Ilija Radosavovic, Raj Prateek Kosaraju, Ross Girshick, Kaiming He, and Piotr Dollár. Designing network design spaces. In *Proceedings of the IEEE/CVF conference on computer vision and pattern recognition*, pages 10428–10436, 2020. 6

[56] Robin Rombach, Andreas Blattmann, Dominik Lorenz, Patrick Esser, and Björn Ommer. High-resolution image synthesis with latent diffusion models. In *Proceedings of the IEEE/CVF conference on computer vision and pattern recognition*, pages 10684–10695, 2022. 2

[57] Chitwan Saharia, William Chan, Huiwen Chang, Chris Lee, Jonathan Ho, Tim Salimans, David Fleet, and Mohammad Norouzi. Palette: Image-to-image diffusion models. In *ACM SIGGRAPH 2022 Conference Proceedings*, pages 1–10, 2022. 2

[58] Mark Sandler, Andrew Howard, Menglong Zhu, Andrey Zhmoginov, and Liang-Chieh Chen. Mobilenetv2: Inverted residuals and linear bottlenecks. In *Proceedings of the IEEE conference on computer vision and pattern recognition*, pages 4510–4520, 2018. 2, 6

[59] Joonghyuk Shin, Minguk Kang, and Jaesik Park. Fill-up: Balancing long-tailed data with generative models. *arXiv preprint arXiv:2306.07200*, 2023. 3

[60] StabilityAI. Stable diffusion public release, 2023. 3

[61] Mingxing Tan, Bo Chen, Ruoming Pang, Vijay Vasudevan, and Quoc V Le. Mnasnet: platform-aware neural architecture search for mobile. *corr abs/1807.11626* (2018). *arXiv preprint arXiv:1807.11626*, 2018. 6

[62] Yonglong Tian, Lijie Fan, Phillip Isola, Huiwen Chang, and Dilip Krishnan. Stablerep: Synthetic images from text-to-image models make strong visual representation learners. *arXiv preprint arXiv:2306.00984*, 2023. 2

[63] Hugo Touvron, Matthieu Cord, Matthijs Douze, Francisco Massa, Alexandre Sablayrolles, and Hervé Jégou. Training data-efficient image transformers & distillation through attention. In *International conference on machine learning*, pages 10347–10357. PMLR, 2021. 7

[64] Xiuying Wei, Ruihao Gong, Yuhang Li, Xianglong Liu, and Fengwei Yu. Qdrop: Randomly dropping quantization for extremely low-bit post-training quantization. *arXiv preprint arXiv:2203.05740*, 2022. 2, 3

[65] Shoukai Xu, Haokun Li, Bohan Zhuang, Jing Liu, Jiezhang Cao, Chuangrun Liang, and Mingkui Tan. Generative low-bitwidth data free quantization. In *Computer Vision–ECCV 2020: 16th European Conference, Glasgow, UK, August 23–28, 2020, Proceedings, Part XII 16*, pages 1–17. Springer, 2020. 1, 2, 7

[66] Kohei Yamamoto. Learnable companding quantization for accurate low-bit neural networks. In *Proceedings of the IEEE/CVF conference on computer vision and pattern recognition*, pages 5029–5038, 2021. 2

[67] Hongxu Yin, Pavlo Molchanov, Jose M Alvarez, Zhizhong Li, Arun Mallya, Derek Hoiem, Niraj K Jha, and Jan Kautz. Dreaming to distill: Data-free knowledge transfer via deep-inversion. In *Proceedings of the IEEE/CVF Conference on Computer Vision and Pattern Recognition*, pages 8715–8724, 2020. 2, 4

[68] Penghang Yin, Jiancheng Lyu, Shuai Zhang, Stanley Osher, Yingyong Qi, and Jack Xin. Understanding straight-through estimator in training activation quantized neural nets. *arXiv preprint arXiv:1903.05662*, 2019. 2, 3

[69] Zhihang Yuan, Chenhao Xue, Yiqi Chen, Qiang Wu, and Guangyu Sun. Ptq4vit: Post-training quantization for vision transformers with twin uniform quantization. In *European Conference on Computer Vision*, pages 191–207. Springer, 2022. 6, 7

[70] Chaoning Zhang, Chenshuang Zhang, Sheng Zheng, Yu Qiao, Chenghao Li, Mengchun Zhang, Sumit Kumar Dam, Chu Myaet Thwal, Ye Lin Tun, Le Luang Huy, et al. A complete survey on generative ai (aigc): Is chatgpt from gpt-4 to gpt-5 all you need? *arXiv preprint arXiv:2303.11717*, 2023. 2

[71] Dongqing Zhang, Jiaolong Yang, Dongqiangzi Ye, and Gang Hua. Lq-nets: Learned quantization for highly accurate and compact deep neural networks. In *Proceedings of the European conference on computer vision (ECCV)*, pages 365–382, 2018. 2

[72] Xiangguo Zhang, Haotong Qin, Yifu Ding, Ruihao Gong, Qinghua Yan, Renshuai Tao, Yuhang Li, Fengwei Yu, and Xianglong Liu. Diversifying sample generation for accurate data-free quantization. In *Proceedings of the IEEE/CVF Conference on Computer Vision and Pattern Recognition*, pages 15658–15667, 2021. 1, 2, 8

[73] Yuxuan Zhang, Huan Ling, Jun Gao, Kangxue Yin, Jean-Francois Lafleche, Adela Barriuso, Antonio Torralba, and Sanja Fidler. Datasetgan: Efficient labeled data factory with minimal human effort. In *Proceedings of the IEEE/CVF Conference on Computer Vision and Pattern Recognition*, pages 10145–10155, 2021. 2

[74] Ritchie Zhao, Yuwei Hu, Jordan Dotzel, Chris De Sa, and Zhiru Zhang. Improving neural network quantization without retraining using outlier channel splitting. In *International conference on machine learning*, pages 7543–7552. PMLR, 2019. 2

[75] Yunshan Zhong, Mingbao Lin, Gongrui Nan, Jianzhuang Liu, Baochang Zhang, Yonghong Tian, and Rongrong Ji. Intraq: Learning synthetic images with intra-class heterogeneity for zero-shot network quantization. In *Proceedings of the IEEE/CVF Conference on Computer Vision and Pattern Recognition*, pages 12339–12348, 2022. 2, 6, 7

[76] Shuchang Zhou, Yuxin Wu, Zekun Ni, Xinyu Zhou, He Wen, and Yuheng Zou. Dorefa-net: Training low bitwidth convolutional neural networks with low bitwidth gradients. *arXiv preprint arXiv:1606.06160*, 2016. 2

StableQ: Enhancing Data-Scarce Quantization with Text-to-Image Data

Supplementary Material

A. Prompt Template

We use the following template to generate the prompt:

1. photo of a {C}.
2. rendering of a {C}.
3. cropped photo of the {C}.
4. the photo of a {C}.
5. photo of a clean {C}.
6. photo of a dirty {C}.
7. dark photo of the {C}.
8. photo of my {C}.
9. photo of the cool {C}.
10. close-up photo of a {C}.
11. bright photo of the {C}.
12. cropped photo of a {C}.
13. photo of the {C}.
14. good photo of the {C}.
15. photo of one {C}.
16. close-up photo of the {C}.
17. rendition of the {C}.
18. photo of the clean {C}.
19. rendition of a {C}.
20. photo of a nice {C}.
21. good photo of a {C}.
22. photo of the nice {C}.
23. photo of the small {C}.
24. photo of the weird {C}.
25. photo of the large {C}.
26. photo of a cool {C}.
27. photo of a small {C}.

B. Patch Similarity

Li *et al.* [40] observed that the multi-head attention in Vision Transformers [16] will generate diverse attention in different patches, especially the foreground and the background of the images. Here, we give a brief introduction to the patch similarity metric.

Formally, given the output features tensor \mathbf{o} , we first calculate the cosine similarity matrices between any two sub-tensors in the patch dimension, given by

$$\Gamma(\mathbf{o}_i, \mathbf{o}_j) = \frac{\mathbf{o}_i \cdot \mathbf{o}_j}{\|\mathbf{o}_i\| \|\mathbf{o}_j\|}, \quad (13)$$

where \mathbf{o}_i denotes the i -th patch of the output featuremap. After calculation, we get the $N \times N$ (N is the #patches) matrix Γ . To measure the diversity of the patch similarities, we calculate differential entropy as follows

$$H = - \int \hat{f}_h(x) \cdot \log[\hat{f}_h(x)] dx. \quad (14)$$

where $\hat{f}_h(x)$ is the continuous probability density function of Γ , which can be obtained by the kernel density estimation [40]. A low entropy value indicates that the patch similarity distribution is less diverse. Hence, we can define a threshold α that only selects the synthetic images where $H > \alpha$.